Nanoscale Horizons

ROYAL SOCIETY OF CHEMISTRY

COMMUNICATION

Published on 05 March 2026
Licence and permissions

Check for updates

Cite this: *Nanoscale Horiz.*, 2026, **11**, 1426

Received 7th December 2025,
Accepted 17th February 2026

DOI: 10.1039/d5nh00796h

rsc.li/nanoscale-horizons

Triboelectricity-driven chemistry at oppositely charged triboelectric interfaces with ionic dyes

Sidra Tul Muntaha,[ab] Tanlin Xu,[c] Shaoxin Li,[ab] Xiang Li,[a] Di Wei *[a] and Zhong Lin Wang [a]

Solid–liquid contact electrification (SL-CE) has emerged as a distinctive pathway for driving interfacial chemistry, yet the principles governing how triboelectric polarity couples with electrolyte identity to regulate reaction activity remain poorly understood. In this study, triboelectricity-driven chemistry at solid–liquid interfaces was examined using two representative materials positioned at far ends of the triboelectric series, and paired with cationic or anionic dyes. It was found that adsorption and the formation of an electrical double layer might result in suppressed interfacial charge transfer, leading to markedly diminished, and in some cases fully inhibited, generation of reactive oxygen species. These findings establish a mechanistic framework for triboelectric polarity–electrolyte coupling, highlighting the pivotal role of surface physicochemical properties in governing SL-CE and offering general design principles for optimizing triboelectricity-driven chemical reactions.

New concepts

This work establishes a surface-governed framework for contact-electrochemistry (CE-Chemistry), demonstrating that charge transfer at solid–liquid interfaces scales with the effective contact area and is critically determined by the interfacial charging behavior of the dielectric in aqueous environments. We reveal that reaction efficiency is not an intrinsic bulk property but is governed by how electrolyte polarity, surface charge, and hydrophobic interactions collectively regulate liquid–solid interface contact and charge transfer. Using model systems, we show that negatively charged surfaces paired with negatively charged electrolytes enhance charge transfer through electrostatic repulsion that improves interfacial wetting, whereas oppositely charged combinations promote ion adsorption that blocks active sites and suppresses electron transfer, in extreme cases leading to complete reaction inhibition. These findings depart from conventional interpretations that emphasize bulk dielectric or mechanical effects, and instead identify dynamic surface charge regulation as the dominant factor controlling contact electrification and reactivity. By unifying contact-area scaling, surface charge effects, and adsorption-mediated blocking into a single conceptual picture, validated across different activation modes such as ultrasound and ball milling, this work provides new mechanistic insight into interfacial charge transfer. The concept offers a rational strategy for tuning contact electrification processes through surface engineering, advancing nanoscience by linking nanoscale interfacial physics directly to macroscopic chemical functionality.

Introduction

Interfacial chemical reactions underpin a broad spectrum of natural and technological processes, and their mechanistic origins have long been a subject of sustained investigation. Photocatalysis and electrocatalysis exemplify established paradigms in which interfacial charge carriers initiate and steer chemical transformations. Recently, triboelectricity-driven contact-electro-chemistry (CE-Chemistry) has emerged as a compelling alternative paradigm, enabling interfacial reactions to proceed in the absence of external irradiation or applied bias.[1] Rooted in mechanically driven solid–liquid contact electrification (SL-CE), CE-Chemistry initiates with interfacial electron transfer, followed by ion migration and electrical double-layer (EDL) formation, while the same electron-transfer process concurrently drives the generation of reactive oxygen species (ROS).[2] These coupled events are governed by the transient electric fields produced during contact and separation.[3] The scope of CE-Chemistry has expanded rapidly, evolving from early demonstrations in pollutant degradation for water treatment to a broad suite of diverse redox transformations,[4,5] polymerization reactions, fluorescence modulation,[6–8] and a growing range of chemical processes in both aqueous and non-aqueous environments,[9–11] along with medical and energy harvesting applications.[12–15] As the field advances, it has become increasingly important to delineate the material, interfacial, and electrolyte parameters that govern CE-Chemistry efficiency and ultimately define the boundaries of its broader chemical potential.[16,17]

[a] *Beijing Institute of Nanoenergy and Nanosystems, Chinese Academy of Sciences, Beijing, 101400, P. R. China. E-mail: weidi@binn.cas.cn*
[b] *School of Nanoscience and Engineering, University of Chinese Academy of Sciences, Beijing, 100049, P. R. China*
[c] *Floor 8, CCHH, United College, The Chinese University of Hong Kong, Hong Kong, China*

This journal is © The Royal Society of Chemistry 2026

CE-Chemistry provides a distinctive framework for elucidating the fundamental mechanisms that govern electron transfer from the liquid phase to solid surfaces.[18] When exposed to the intense localized pressures and temperatures generated by ultrasound, reactive aqueous environments synergistically accelerate interfacial electron-transfer processes, enabling efficient contact-electro-catalysis (CEC) through the generation of ROS. Despite the recent surge of interest in solid–water interfacial phenomena, the fundamental principles governing CEC remain at an early stage, underscoring the need for a deeper mechanistic understanding of solid–liquid interactions. Although electron transfer is central to CEC and ostensibly shared across materials, no study has yet provided a comprehensive comparison of rate kinetics or catalytic efficiencies among different triboelectric materials. Only a few reports have examined EDL formation in aqueous CEC systems, despite its likely impact on reaction kinetics.[16,19,20] Likewise, mechanistic insights remain limited to studies that modulate surface functional groups, with far fewer investigations exploring material substitution, fluorination of non-fluoropolymers, or the rate constants associated with fully fluorinated materials.[21–24] Recent literature indicates that electron transfer in SL-CE is governed not only by the intrinsic triboelectric series of materials but also by the dynamic configuration of the interfacial EDL.[25–29] However, the direct measurement of the EDL under mechanically driven, transient conditions remains experimentally challenging, leaving unresolved how the charge polarity of the solid surface and the ionic composition of the contacting electrolyte jointly regulate charge transfer, ROS generation, and overall reaction kinetics.

In this study, we interrogate the fundamental role of charge polarity by systematically comparing triboelectric materials spanning opposite ends of the triboelectric series and surface functional groups to elucidate how dielectric charge and electrolyte ion polarity co-govern CE-Chemistry. To our knowledge, this is the first study to systematically interrogate solid dielectrics selected from the extreme ends of the triboelectric series in combination with electrolytes containing either cationic or anionic species, thereby revealing how surface adsorption and the resulting interfacial EDL structure collectively govern reaction kinetics. We first quantified the intrinsic charge density of each dielectric using a triboelectric nanogenerator (TENG), then determined the charge generated at solid–liquid interfaces using a water-droplet TENG configuration to establish the polarity and magnitude of charge transfer during dielectric solid–water contact. These materials were subsequently evaluated in an ultrasound-driven CE-Chemistry process, allowing direct comparison of their charge generation under water, adsorption behavior, and catalytic performance toward cationic or anionic charged dyes, as well as their activity on surfaces with inverse polarity during ball-milling catalysis. Collectively, this work establishes a mechanistic insight linking adsorption, EDL structure, and surface charge polarity to CE-Chemistry reaction kinetics, offering a new framework for the rational design of triboelectric triggered reactions.

Results and discussion

Charging behavior in contact electrification

A central mechanistic question in CE-Chemistry is how contact electrification (CE) at the interfaces of polytetrafluoroethylene (PTFE), polyamide 6,6 (PA-66), translates into measurable catalytic activity. Although interfacial electron transfer and charge separation constitute the primary origin of CE, the resulting catalytic output arises from the coupled effects of the excitation mode, the hydrophobic or hydrophilic nature of the surface, the structure of the EDL, and the polarity and magnitude of the surface charge. In this section, the influence of solid–solid contact on the initial charge density is elucidated, and the manner in which this interfacial charge governs EDL formation and, ultimately, the efficiency of CE-driven reaction pathways is examined.

Fig. 1a and b shows the molecular structures of PTFE and PA-66, two polymers deliberately selected from opposite extremes of the triboelectric series to enable a systematic investigation of how triboelectric polarity couples to electrolyte identity in SL-CE. PTFE, enriched with highly electronegative $-CF_2$ groups, exhibits a strong electron-accepting character and thus resides near the most negative end of the triboelectric series. By contrast, PA-66 contains electron-donating amide (–CONH–) functionalities, positioning it at the positive end. Both polymers also display strikingly different behaviour when immersed in an aqueous electrolyte. Under neutral pH conditions ($\sim$6–8), both materials acquire a net negative surface charge, consistent with their well-established isoelectric points (IEP): $\sim$3 for PTFE[30–33] and $\sim$4–5 for PA-66.[34] Above these pH thresholds, deprotonation and interfacial electron transfer yield negatively charged surfaces that develop classical EDLs comprising counter-ion enrichment in the Stern layer.

Faraday-cup measurements (Fig. 1c and d) confirm this behaviour quantitatively. Upon repeated contact, water consistently emerges with a net positive charge, while the solid surfaces accumulate negative charge. The magnitude of this charge transfer varies systematically with the dielectric: PTFE generates the largest negative charge ($\sim$0.30 nC per cycle), followed by PA-66 ($\sim$0.15 nC), reflecting their relative positions in the triboelectric series and their interfacial electron-accepting propensities. Together, these measurements establish a clear hierarchy of triboelectric charge acquisition in aqueous media: PTFE > PA-66, and demonstrate that dielectrics drawn from opposite ends of the triboelectric series retain distinct and predictable charging behaviour even under aqueous solid–liquid contact.

Fig. 1g presents a schematic illustrating the electrical double layer (EDL) formation at the dielectric solid–liquid interface. It is important to recognize that surface wettability plays a determinative role in interfacial charge-transfer pathways. Relatively hydrophobic surfaces preferentially promote electron transfer, whereas hydrophilic surfaces facilitate ion transfer due to stronger interfacial interactions and more pronounced EDL formation. This tunable material contrast provides a mechanistic foundation for systematically analyzing how triboelectric polarity, surface wettability, interfacial adsorption, and

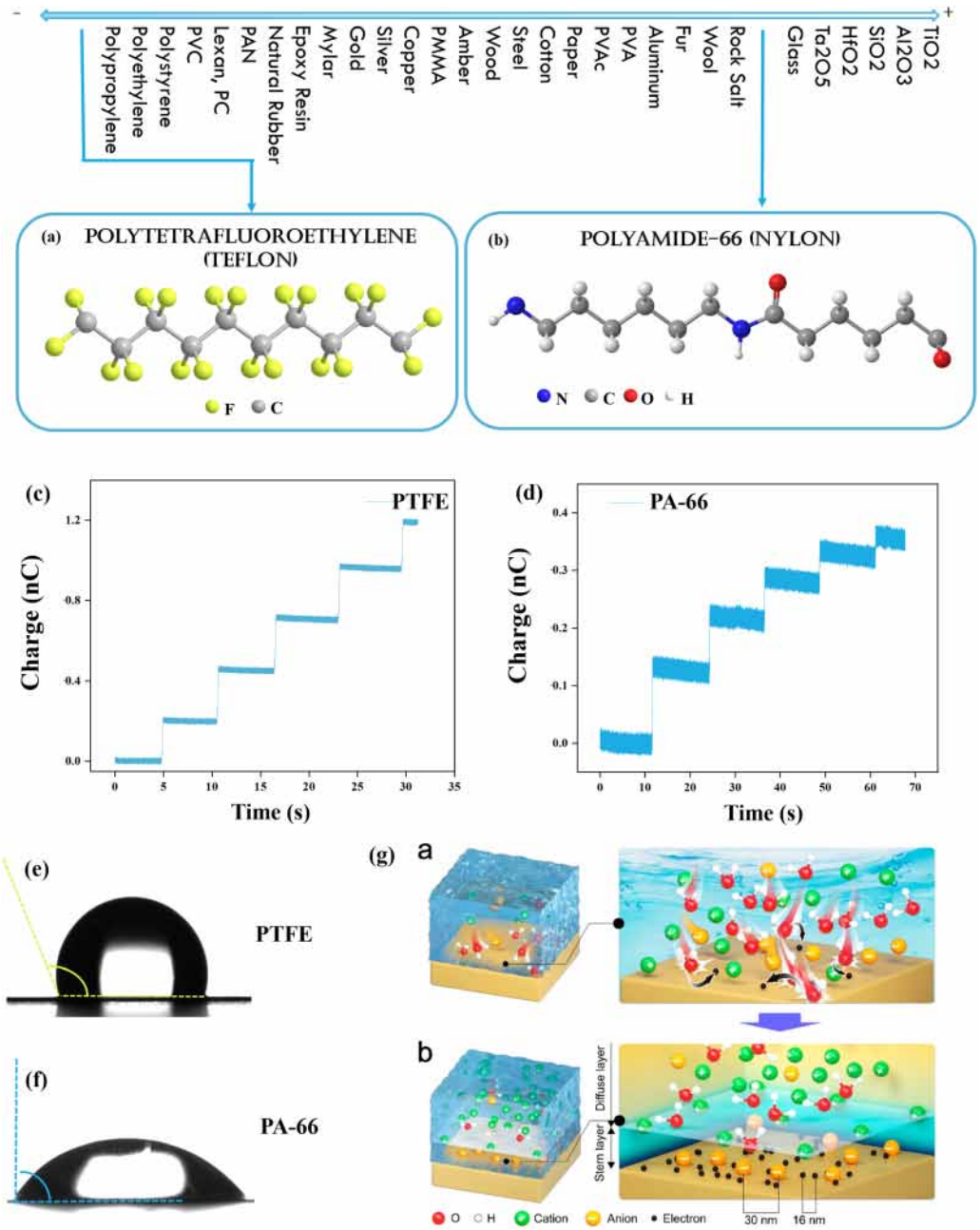


Fig. 1 Molecular structures of (a) PTFE and (b) PA-66. Charge transfer measurement between water and (c) PTFE and (d) PA-66. Contact angle of water with (e) PTFE and (f) PA-66. (g) Wang's two-step EDL, model and its formation processes. (a) In the first step, electron transfer occurs between the liquid and the solid, while ions might also adsorb onto the solid surface. (b) In the second step, free ions in the liquid are attracted to the charged solid surface due to electrostatic interactions. Reproduced with permission from American Chemical Society (2022).[38]

EDL structure collectively govern CE-Chemistry reaction kinetics.[35–38]

Quantifying the density of triboelectric charges

To quantify the triboelectric charge, films with a surface area of 2.5 cm^2 were prepared from three dielectrics materials, with a copper electrode laminated beneath each film to serve as the charge-collecting layer (Fig. S2). To establish the intrinsic charge characteristics of PTFE and PA-66, the triboelectric charge density generated under controlled solid–solid and solid–liquid contact was then systematically quantified. These measurements form the foundation for understanding how surface polarity and charge magnitude regulate subsequent adsorption behavior, EDL formation, and CE-Chemistry reaction kinetics. Fig. 2 summarizes the experimental configurations and the resulting charge outputs. Fig. 2a and b positions these materials along the triboelectric series: PTFE lies at the strongly negative end and PA-66 at the strongly positive end. This ordering defines the expected direction of electron transfer during contact and establishes an essential framework for

 This journal is © The Royal Society of Chemistry 2026

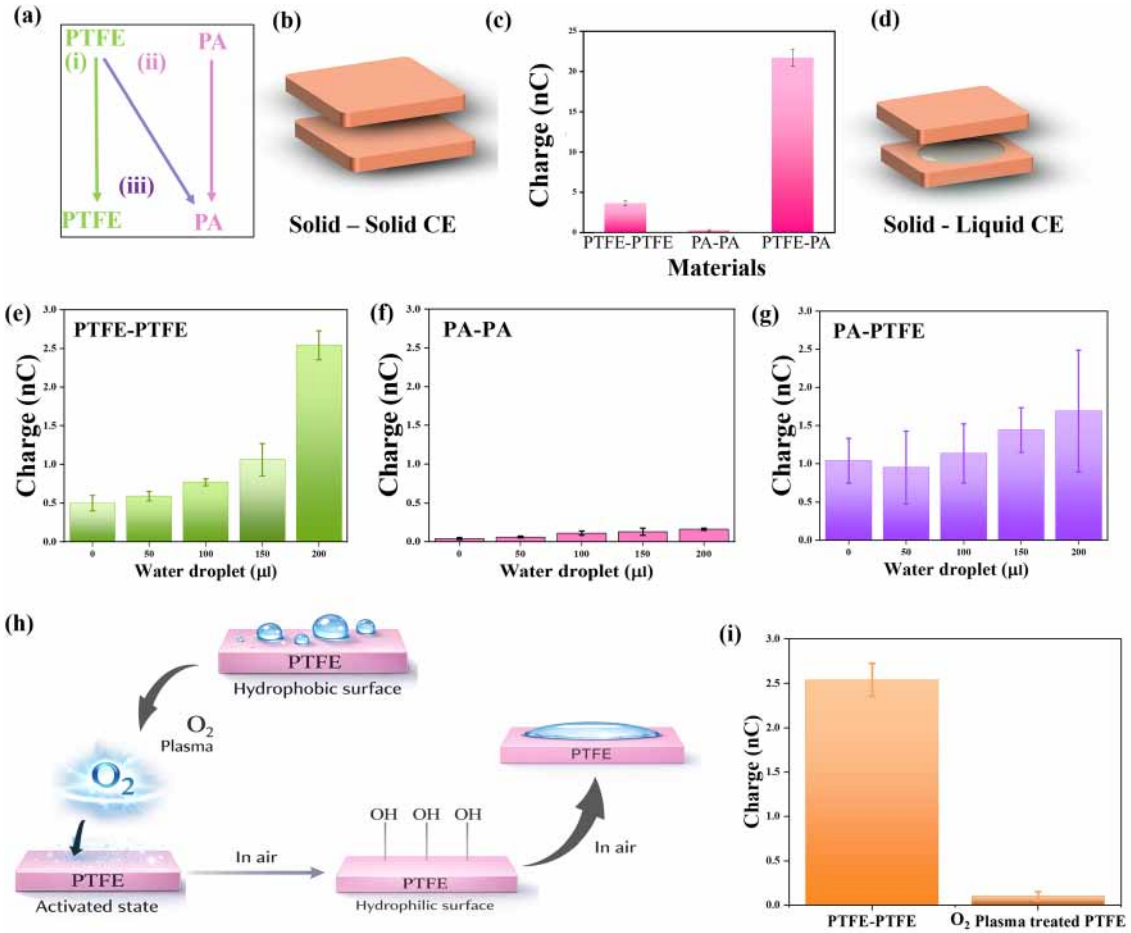


Fig. 2 (a) Solid–solid and solid–liquid contact electrification between different materials. (b) A visual illustration of solid–solid CE. (c) Bar chart showing the amount of charge transferred between different dielectric films. The red wire was attached to PA in PTFE–PA CE. (d) A visual illustration of SL-CE. SL-CE between two dielectric films in the presence of different amounts of water droplets: (e) PTFE–PTFE, (f) PA–PA and (g) PA–PTFE. (h) Schematic of the PTFE surface before and after oxygen plasma treatment. (i) Charge transfer measurement between PTFE–PTFE and oxygen plasma treated PTFE–PTFE slabs.

interpreting catalytic behavior that is further discussed in the upcoming sections. To quantify solid–solid charge generation, a vertical contact-separation triboelectric nanogenerator (TENG) configuration was used (Fig. 2b and Fig. S1). Repeated mechanical contact induces interfacial electron transfer, generating opposite charges on the two surfaces. Fig. 2c shows the resulting charge densities for each pairwise contact. As anticipated from the triboelectric series, PTFE–PA interactions yield the highest charge output due to their extreme polarity contrast.

To probe solid–liquid interfacial charge transfer, a key step in CE-Chemistry in aqueous systems, we employed a droplet-based solid–liquid TENG (Fig. 2d). In this configuration, water droplets repeatedly impact and detach from the dielectric surface, allowing direct quantification of the charge transferred during each event. This method captures the polarity and magnitude of electron exchange between the dielectric and water, providing insights into how CE initiates EDL formation in aqueous environments. Water droplets of varying volumes (0, 50, 100, 150, and 200 μL) were introduced between the two surfaces at a fixed separation distance of 1 mm during contact. Increasing the droplet volume led to a proportional increase in the measured triboelectric charge, an effect attributed to the enlarged effective contact area between water and the dielectric surface. The measured triboelectric output for water contacting PTFE and PA-66 is shown in Fig. 2e–g. Water consistently acquires a net positive charge, while all solid surfaces become negatively charged, confirming an electron-donating tendency from water to the dielectric in the case of SL-CE. Among the materials, PTFE exhibits the highest negative charge transfer, followed by PA-66. These trends correlate with their hydrophobicity and their relative positions along the triboelectric series, demonstrating that intrinsic surface chemistry governs the extent of solid–water electron transfer. The statistical distributions of charge output across repeated cycles further underscore these differences. PTFE showed the highest and most consistent charge density, reflecting its strong electron-accepting nature. PA-66 exhibited intermediate values with moderate variability. Collectively, these comparisons confirm that triboelectric charge density arises from the coupled effects of surface polarity, chemical functionality, and wettability.

Furthermore, the PTFE surface was subjected to oxygen plasma treatment to deliberately tailor its surface chemistry

and interfacial properties. Oxygen plasma etching introduces polar oxygen-containing functional groups, particularly hydroxyl (–OH) species, onto the otherwise chemically inert PTFE surface through bond scission and surface activation, as schematically illustrated in Fig. 2h. This modification markedly increases the surface energy and alters wettability, transforming the initially hydrophobic PTFE into a more hydrophilic interface. The change in wettability is corroborated by contact-angle measurements obtained before and after plasma treatment, as shown in Fig. S4.

The incorporation of hydroxyl functionalities increases the surface affinity toward polar liquid molecules and strengthens interfacial interactions, thereby promoting ion adsorption and facilitating EDL formation. Experimentally, this effect is manifested as a pronounced reduction in the measured charge, decreasing from ~2.5 nC for untreated PTFE to ~0.1 nC after oxygen plasma treatment, as shown in Fig. 2i. This result underscores the critical role of surface chemical functionality and wettability in governing the CE process.

Furthermore, the deliberate structuring of the EDL at the interface is not only central to the fundamental charge transfer process but can also be harnessed to significantly boost triboelectric output. For instance, engineering ion gradients to create EDL-mediated charge separation has been shown to dramatically enhance the performance of triboelectric nanogenerators by reducing charge screening.[39,40] This underscores the practical importance of EDL dynamics in optimizing systems reliant on triboelectrification.

Overall, this section establishes a quantitative foundation for linking triboelectric charge density to downstream interfacial phenomena. The systematic variation across dielectrics demonstrates how intrinsic surface properties shape initial charge separation, which in turn dictates EDL formation, adsorption of charged species, and the ability of each dielectric to drive CE-Chemistry under ultrasound or mechanical excitation, as discussed in the following sections.

Ultrasound-driven CE-Chemistry performance with cationic and anionic dyes

To evaluate CE-Chemistry under realistic water-treatment conditions, we investigated the degradation of two structurally and electronically distinct dyes, methyl orange (MO, an anionic dye) and Basic Blue 41 (CB, a cationic dye), under ultrasonic excitation (Fig. 3a). While most CE-Chemistry studies have focused exclusively on anionic dyes,[41,42] the inclusion of a cationic analogue enables direct assessment of how interfacial charge polarity governs CE-driven reactivity. Under ultrasound irradiation alone, no measurable degradation was observed at 120 W, while CB underwent approximately 70% degradation at 500 W (Fig. 3b); radical-scavenger experiments (Fig. S7) confirmed that this process is mediated by ultrasound-induced ROS rather than direct cavitation-driven cleavage. To investigate how dielectric surfaces modulate this behaviour, PTFE and PA-66 (4 mm) were introduced as triboelectric interfaces capable of initiating CE and enhancing ROS generation.

PTFE, located at the negative extreme of the triboelectric series, markedly accelerated dye degradation: at 500 W, both dyes were fully degraded within one hour (Fig. 3c and d), whereas at 120 W, MO degraded within two hours and CB remained only partially degraded after four hours (Fig. 3e and

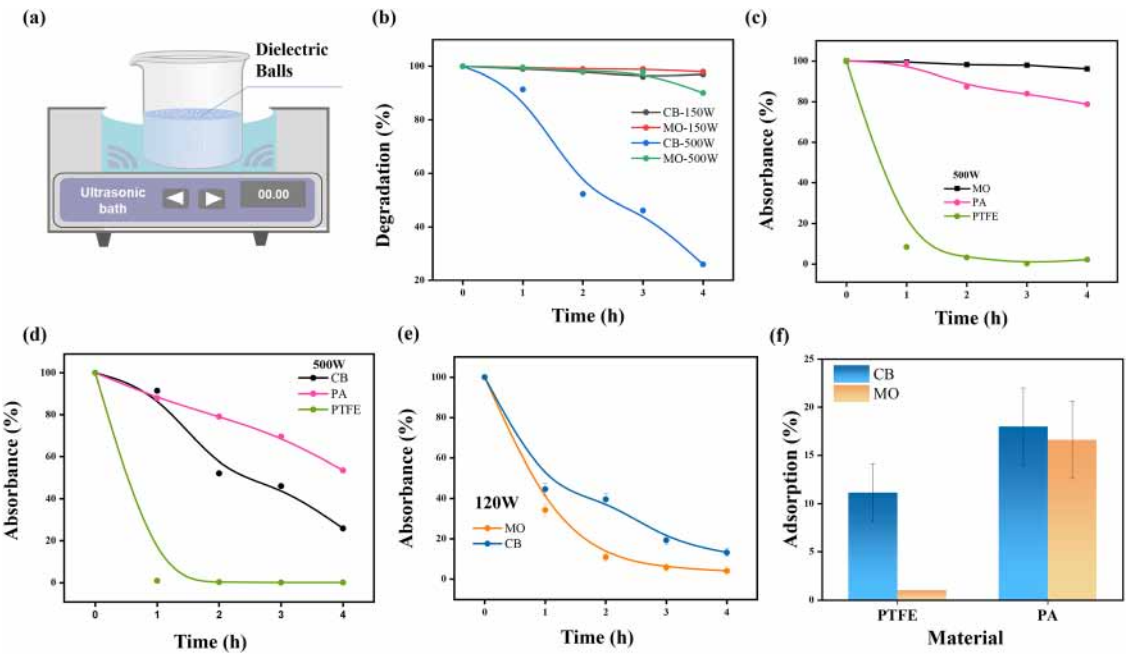


Fig. 3 (a) Illustration of the experimental setup comprising a power circulator that regulates the power of the reactor and an ultrasonic bath (40 kHz, 120–500 W). (b) Degradation of MO and CB at 120 W and 500 W ultrasonic power. Evolution of the relative absorbance of (c) MO and (d) CB in the presence of different dielectric materials at 500 W. (e) Evolution of the relative concentration of MO and CB in the presence of PTFE at 120 W. (f) Adsorption percentage of MO and CB on the surface of different dielectric materials for a period of 4 h under static conditions.

 This journal is © The Royal Society of Chemistry 2026

Table S1). This polarity-dependent behaviour arises from the fundamentally different interfacial interactions experienced by each dye. For CB, the electrostatic attraction between the cationic aromatic chromophore and the negatively charged PTFE surface might perturb the interfacial EDL, drawing dye molecules into the vicinity of the Stern layer and thereby diminishing the accessibility of ROS generated in the aqueous phase. In contrast, MO, an anionic dye, experiences electrostatic repulsion from PTFE, which suppresses surface adsorption, preserves interfacial water structure, and enables more efficient ROS-mediated oxidative decomposition. A more detailed consideration of CB's molecular architecture further rationalizes its suppressed degradation. CB is a monomeric cationic azo dye comprising two conjugated aromatic rings linked by an –N═N– bridge: a benzothiazolium ring (bearing methyl and methoxy substituents) that hosts the formal positive charge (shown in Fig. S6), and a phenyl ring substituted with an *N*-ethyl-2-hydroxyethylamino group. This molecular framework combines extensive π-conjugation, hydrophobic aromatic domains capable of π–π or hydrophobic interactions, and polar heteroatoms (N, O, and S) that serve as hydrogen-bond acceptors, alongside a single hydrogen-bond donor (–OH). Such mixed hydrophobic character could enable CB to engage strongly with hydrophobic polymer surfaces such as PTFE. The intimate association between the dye's aromatic rings and the fluorinated PTFE backbone likely reinforces adsorption through van der Waals and hydrophobic interactions, effectively sequestering CB at the solid interface. This adsorption might not only reduce the effective concentration of freely solvated CB but also decrease the interfacial area accessible for electron exchange between water and PTFE. As a consequence, the interfacial triboelectric field and ROS flux could become insufficient to disrupt CB's conjugated structure, thereby significantly attenuating its degradation kinetics.

PA-66, despite developing a negative surface charge in water similar to PTFE, exhibits fundamentally different interfacial behaviour and entirely suppresses the degradation of both dyes at all ultrasound intensities. This inhibition might arise from its strong, nonspecific adsorption capacity, enabled by the amide and carbonyl functionalities on the PA backbone, which effectively mask the surface, block CE-induced charge transfer, and quench ROS formation. Both PA balls and PA films demonstrated identical suppression (Fig. S9), highlighting that the effect originates from intrinsic surface chemistry rather than particle morphology. For CB, a cationic aromatic dye, electrostatic attraction to the negatively charged PA surface drives strong adsorption. Unlike PTFE, where adsorption is confined to the interfacial region, PA exhibits pronounced internal diffusion. Sectioned PA balls reveal CB penetration to ~2 mm depth, indicating that dye molecules diffuse into the polymer matrix rather than remaining surface-bound. Our recent findings show that CE-Chemistry performance is governed by the nature of the functional groups on the outermost surface of the dielectric. After fluorinating a silicon surface, its solid–liquid CE behaviour becomes identical to that of fluorinated dielectric materials.[22] This bulk uptake also dramatically reduces the available interfacial area for CE-mediated electron exchange, resulting in near-complete loss of ROS production and suppression of CB degradation, which otherwise reaches ~70% in the absence of PA. Thus, internal diffusion within PA, not merely surface adsorption, is a dominant factor inhibiting CE-Chemistry. MO, though anionic, exhibits a similarly strong adsorption on PA despite the absence of π–π interactions, as PA is not an aromatic polymer. Instead, MO binds through hydrogen bonding and electrostatic interactions facilitated by heteroatoms in its structure and its pK_a of 3.4, which allows partial ionization under neutral conditions.[34,43,44] The dimethyl-substituted nitrogen and the sulfonate-bearing sulfur atom serve as active binding sites (Fig. S5). Ultrasound irradiation further enhances dye uptake by promoting diffusion and transient pore opening, driving PA into an adsorption-dominated regime that suppresses ROS formation for MO as well.[45] Taken together, these results reveal that ultrasound-activated CE-Chemistry is governed by a coupled interplay between dielectric charge polarity, hydrophobicity, dye-surface adsorption, and interfacial dynamics. While PTFE's hydrophobic surface primarily modulates CE efficiency through interfacial adsorption and EDL restructuring, PA exerts a more profound inhibitory effect by removing dye molecules from the reactive zone through both surface binding and bulk absorption. These findings highlight that surface physicochemical properties, not only triboelectric polarity, serve as decisive determinants of CE-Chemistry efficiency in aqueous systems, and that rational tuning of dielectric surface chemistry is essential for optimizing triboelectric catalytic performance.

To further elucidate the role of adsorption as an inhibiting factor in CB degradation, PA spheres previously exposed to CB and methyl orange solutions were removed and immersed in fresh deionized (DI) water. After standing overnight, the DI water developed a faint blue coloration, indicating desorption of CB from the PA surface into the surrounding medium. The recovered solution was analyzed using UV-vis spectroscopy, and the absorption profile was found to be consistent with that of pristine CB, confirming that no structural or chemical transformation had occurred during adsorption (Fig. S12). A similar desorption behavior and spectral response were observed for methyl orange.

These findings indicate that the reduced degradation efficiency in the presence of PA-66 might be primarily governed by strong dye adsorption onto the polymer surface. The formation of an adsorbed dye layer likely occupies and shields active interfacial sites, thereby impeding effective charge transfer and suppressing the electron exchange processes required for efficient degradation. As CE-Chemistry is fundamentally an interfacial phenomenon, its performance is governed by the triboelectric characteristics of the outermost surface molecular structure; surface coverage by adsorbates can therefore directly weaken charge generation and diminish the interfacial driving force for reaction.[22]

To assess the operational stability and reusability of the PTFE balls under sustained catalytic cycles, we examined the balls after 5 consecutive reaction cycles (each cycle consisting of

four hours) (Fig. S13). No visible signs of surface degradation, physical wear, or fouling were observed by optical microscopy, except for the adsorbed dye molecules on the PTFE surface. The images before and after five consecutive cycles are included in Fig. S14.

Ball-milling activation of CE-chemistry

Ball milling was explored as an alternative mechano-activation platform[46] for CE-Chemistry, offering a cavitation-free environment distinct from ultrasound systems, where bubble collapse generates extreme local temperatures and pressures. Fig. 4a shows a schematic of the liquid-assisted ball-milling process, highlighting the repeated impacts between the milling balls and the PTFE vial that generate triboelectric charge and facilitate interfacial reactions. The calculated collision frequencies, kinetic energies, and collision powers for the Retsch PM 100 system (Fig. S15 and Table S4) show that, at identical rotation speeds, PTFE balls deliver the highest impact energies owing to their greater mass and high Young's modulus (Tables S2 and S3), thereby generating more forceful triboelectric interactions than PTFE or PA.

In CE-Chemistry experiments, 50 mL of a 5 ppm MO or CB solution was milled with 1200 balls composed of PTFE and PA at 360 rpm for 4 h using intermittent milling cycles (7 min milling/3 min rest) to minimize temperature rise. The subsequent UV-vis spectra showed the evolution of MO concentration in the presence of different dielectrics: PTFE balls (Fig. 4b) induce rapid spectral decay indicative of efficient degradation *via* triboelectric charge. PA (Fig. 4c) causes substantial spectral attenuation arising primarily from adsorption rather than oxidative breakdown. PA-66 exhibited pronounced dye–surface interactions, as evidenced by the substantial attenuation of MO and CB absorbance signals shown in Fig. 4c and Fig. S19. The decreases of 30% and 70%, respectively, arise from strong electrostatic binding between the dye molecules and the amide functionalities on PA, as discussed in section "Ultrasound-driven CE-Chemistry performance with cationic and anionic dyes". Given the large accessible surface area of the 1200 milling balls ($\sim$60 319 mm^2; Fig. S17, S18 and 20), adsorption is extensive, resulting in the formation of a thick layer of adsorbed dye at the surface that might suppress charge transfer and inhibit ROS generation. This behavior mirrors that observed under ultrasound excitation, where PA likewise suppressed CE-Chemistry through strong, nonspecific adsorption.

A consolidated comparison of MO absorbance across all dielectrics (Fig. 4d) highlights the strong dependence of dye depletion on surface chemistry and polarity, distinguishing ROS-mediated degradation (PTFE) from adsorption-driven attenuation (PA). Degradation profiles for MO and CB in the presence of PTFE balls (Fig. 4e) show rapid degradation of MO but significantly slower degradation of CB, attributable to preferential adsorption of the cationic dye onto PTFE surfaces (Fig. S16 and S17). This adsorption reduces the concentration of free dye and promotes the formation of an interfacial EDL that restricts electron transfer from water to the PTFE surface, consistent with the degradation rates listed in Table S5.

The significantly higher process efficiency of ultrasonication compared with liquid-assisted ball milling (Fig. 4f) can be attributed, in part, to the direct generation of triboelectric charges and the formation of physical liquid jets under

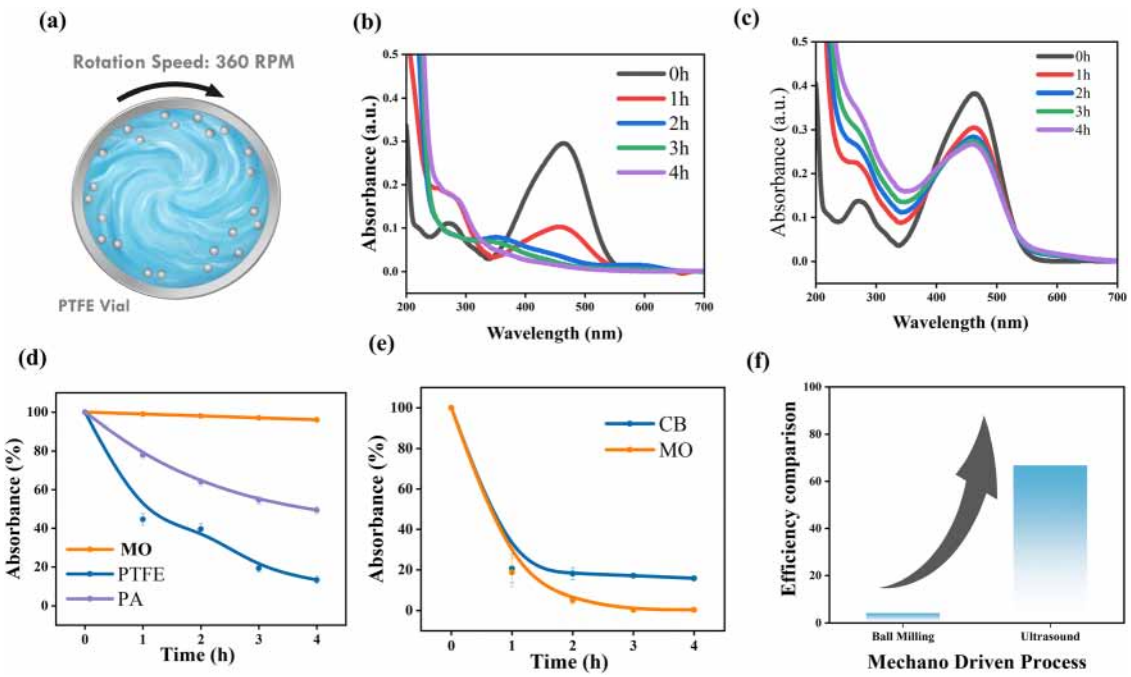


Fig. 4 (a) A visual illustration of a liquid-assisted ball milling process. UV-vis absorption spectra of MO in the presence of (b) PTFE and (c) PA. (d) Comparison of MO absorbance in the presence of various dielectrics. (e) Comparison of MO and CB degradation in the presence of PTFE balls. (f) Efficiency comparison of two mechano-driven processes, ball milling and ultrasound, for the degradation of dyes.

 This journal is © The Royal Society of Chemistry 2026

ultrasonic irradiation, a principle similarly exploited in ultrasound-driven triboelectric energy harvesters.[47]

Conclusion

This work establishes a previously unrecognised mechanistic insight into triboelectricity-driven chemistry by revealing how triboelectric polarity and electrolyte charge jointly govern interfacial electron transfer, EDL formation, and ROS generation at solid–liquid interfaces. By systematically pairing dielectrics positioned at opposite ends of the triboelectric series with cationic and anionic dyes, we demonstrate that strong adsorption governs EDLs, which suppress CE-driven reactivity and, in some cases, can even inhibit the production of ROS. Through complementary mechano-activation pathways, including ultrasound- and liquid-assisted ball milling, we further show that the efficiency, selectivity, and even the reaction mechanism depend sensitively on the interplay between surface polarity, interfacial structure, and dye adsorption energetics. These findings reveal a unifying principle: CE-Chemistry is fundamentally polarity-regulated. By establishing how triboelectric charge density and EDL configuration dictate reaction kinetics across disparate mechanical excitation modes, this study provides the first generalized design rules for engineering triboelectric interfaces for chemical transformations. More broadly, the mechanistic insights presented here open new opportunities for rational control of triboelectricity-driven catalysis, pollutant remediation, interfacial redox processes, and mechano-chemical energy conversion, thereby advancing CE-Chemistry toward a predictive and tunable reaction paradigm.

Author contributions

Sidra Tul Muntaha: data curation, formal analysis, investigation, methodology, and writing original draft. Tanlin Xu and Shaoxin Li: conceptualization, methodology, and visualization. Xiang Li: resources, software, and funding acquisition. Di Wei: project administration, resources, validation, supervision, writing, review and editing, and funding acquisition. Zhong Lin Wang: project administration and funding acquisition.

Conflicts of interest

The authors declare that they have no known competing financial interests or personal relationships that could have appeared to influence the work reported in this paper.

Data availability

The data supporting this article have been included as part of the supplementary information (SI). Supplementary information is available. See DOI: https://doi.org/10.1039/d5nh00796h.

Further raw data will be made available or provided on demand.

Acknowledgements

This work was supported by the National Natural Science Foundation (grant no. 22479016) and China Postdoctoral Science Foundation (certificate no. 2025M781041). During the preparation of this work, the authors used ChatGPT in order to improve the readability and language of the manuscript. After using this tool, the authors reviewed and edited the content as needed and take full responsibility for the content of the publication.

References

1 Z. Wang, X. Dong, W. Tang and Z. L. Wang, Contact-electrocatalysis (CEC), *Chem. Soc. Rev.*, 2024, **53**(9), 4349–4373.
2 S. Li, J. Liu, Z. L. Wang and D. Wei, Mechano-driven chemical reactions, *Green Energy Environ.*, 2024, **10**(5), 937–966.
3 Y. Zhao, *et al.*, The process of free radical generation in contact electrification at solid-liquid interface, *Nano Energy*, 2023, **112**, 108464.
4 S. Li, Z. Zhang, P. Peng, X. Li, Z. L. Wang and D. Wei, A green approach to induce and steer chemical reactions using inert solid dielectrics, *Nano Energy*, 2024, **122**, 109286.
5 M. Shah *et al.*, Synergistic Effects in Triboelectric Charge-Driven Redox Reactions, available at SSRN 5338070.
6 C. Xu, S. Li, Y. Zhang, Z. Wang, Z. L. Wang and D. Wei, Contact-electro-chemistry induced by flow electrification in dielectric tubes, *Nano Energy*, 2025, **134**, 110526.
7 X. Huo, S. Li, B. Sun, Z. Wang and D. Wei, Revealing the Role of Interfacial Charge Transfer in Mechanoluminescence, *Nanomaterials*, 2025, **15**(9), 656.
8 C. Xu, S. Li, Z. Yang, M. Willatzen, Z. L. Wang and D. Wei, Contact-electro-luminescence triggered by triboelectric charge, *Chem. Eng. J.*, 2024, **501**, 157754.
9 X. Huo, S. Li, B. Sun, Z. L. Wang and D. Wei, Recent Progress of Chemical Reactions Induced by Contact Electrification, *Molecules*, 2025, **30**(3), 584.
10 J. Liu, *et al.*, Nonaqueous contact-electro-chemistry via triboelectric charge, *J. Am. Chem. Soc.*, 2024, **146**(46), 31574–31584.
11 T. Gan, *et al.*, Unveiling Janus Chemical Processes in Contact-Electro-Chemistry through Oxygen Reduction Reactions, *J. Am. Chem. Soc.*, 2025, **147**, 25407–25416.
12 P. Zhuang, *et al.*, Solid-Liquid Interface Lubricating Hydrogels for Tendon-Bone Healing, *Research*, 2025, **8**, 0924.
13 X. Wang, A. P. Ivanov and J. B. Edel, Biocompatible Biphasic Iontronics Enable Neuron-Like Ionic Signal Transmission, *Research*, 2024, **7**, 0294.
14 X. Tao, *et al.*, High-Performance Constant Current Triboelectric Nanogenerator for Wind Energy Harvesting and Air Purification, *SmartSys*, 2025, **1**(4), e70012.
15 F. Dong, C. Han, S. T. Cai, J.-H. Lee and S. Niu, Skin-Integrated Wearable Electronics: A Dual-Interface Perspective, *SmartSys*, 2025, **1**(4), e70013.
16 X. Li and W. Tong, Contact-electro-catalysis under natural and industrial conditions: mechanisms, strategies, and challenges, *J. Mater. Chem. A*, 2024, **12**(31), 19783–19805.

17 M.-N. Liu, *et al.*, Strategies for Improving Contact-Electro-Catalytic Efficiency: A Review, *Nanomaterials*, 2025, **15**(5), 386.

18 S. T. Muntaha, Z. L. Wang and D. Wei, Reevaluating Mechano-driven Chemical Reactions: Insights from Ultrasonic, Piezo, and Contact-Electro Mechanisms, *Electrochim. Acta*, 2025, 147563.

19 X. Li, Y. Wei, Z. L. Wang and D. Wei, Iontronic Regulation of Nanoconfined Electrical Double Layers on Dielectric Solids, *Small Sci.*, 2025, **5**(11), 2500371.

20 X. Li, Z. L. Wang and D. Wei, Iontronic logic control driven by dynamic electrical double layer regulation, *Iontronics*, 2025, **1**(1), 2.

21 Y. Su, A. Berbille, Z. L. Wang and W. Tang, Water-solid contact electrification and catalysis adjusted by surface functional groups, *Nano Res.*, 2024, **17**(4), 3344–3351.

22 T. Gan, *et al.*, Sustainable Fluorinated Silicon Dielectric Design for Enhanced Contact-Electro-Chemistry, *Angew. Chem.*, 2025, e202517059.

23 Z. Wang, X. Dong, F.-J. Lv and W. Tang, A perspective on contact-electro-catalysis based on frontier molecular orbitals, *Mater. Adv.*, 2024, **5**(16), 6373–6377.

24 J. Liu, *et al.*, Modular contact-electro-chemistry based on dielectrics with work function-tunable metal coatings, *Nano Energy*, 2025, **144**, 111389.

25 S. Lin, M. Zheng and Z. L. Wang, Detecting the liquid–solid contact electrification charges in a liquid environment, *J. Phys. Chem. C*, 2021, **125**(25), 14098–14104.

26 F. Zhan, *et al.*, Electron transfer as a liquid droplet contacting a polymer surface, *ACS Nano*, 2020, **14**(12), 17565–17573.

27 J. Wu, J. Cao, H. Bi, J. Zhang and Q. Cao, Liquid-solid contact electrification and its effect on the formation of electric double layer: An atomic-level investigation, *Nano Energy*, 2023, **111**, 108442.

28 S. Xiao, *et al.*, Triboelectric mechanism of oil-solid interface adopted for self-powered insulating oil condition monitoring, *Adv. Sci.*, 2023, **10**(13), 2207230.

29 P. Peng, Z. L. Wang and D. Wei, Modulating multi-ion dynamics for high-performance iontronic systems, *Iontronics*, 2026, **2**(1), 5.

30 R. Zimmermann, S. Dukhin and C. Werner, Electrokinetic Measurements Reveal Interfacial Charge at Polymer Films Caused by Simple Electrolyte Ions, *J. Phys. Chem. B*, 2001, **105**(36), 8544–8549.

31 J. Lützenkirchen, T. Preočanin and N. Kallay, A macroscopic water structure based model for describing charging phenomena at inert hydrophobic surfaces in aqueous electrolyte solutions, *Phys. Chem. Chem. Phys.*, 2008, **10**(32), 4946–4955, DOI: 10.1039/B807395C.

32 A. Barišić, J. Lützenkirchen, G. Lefévre and T. Begović, The influence of temperature on the charging of polytetrafluoroethylene surfaces in electrolyte solutions, *Colloids Surf., A*, 2019, **579**, 123616.

33 M. D. Sosa, *et al.*, Liquid–polymer triboelectricity: chemical mechanisms in the contact electrification process, *Soft Matter*, 2020, **16**(30), 7040–7051, DOI: 10.1039/D0SM00738B.

34 K. Wang, *et al.*, Comparing the adsorption of methyl orange and malachite green on similar yet distinct polyamide microplastics: Uncovering hydrogen bond interactions, *Chemosphere*, 2023, **340**, 139806.

35 S. Lin, L. Xu, A. Chi Wang and Z. L. Wang, Quantifying electron-transfer in liquid-solid contact electrification and the formation of electric double-layer, *Nat. Commun.*, 2020, **11**(1), 399.

36 Y. Jin, *et al.*, How liquids charge the superhydrophobic surfaces, (in eng), *Nat. Commun.*, 2024, **15**(1), 4762.

37 Y. Jin, *et al.*, How liquids charge the superhydrophobic surfaces, *Nat. Commun.*, 2024, **15**(1), 4762.

38 S. Lin, X. Chen and Z. L. Wang, Contact Electrification at the Liquid–Solid Interface, *Chem. Rev.*, 2022, **122**(5), 5209–5232.

39 J. Chun, *et al.*, Boosted output performance of triboelectric nanogenerator via electric double layer effect, *Nat. Commun.*, 2016, **7**(1), 12985.

40 Y. Wei, X. Li, Z. Yang, J. Shao, Z. L. Wang and D. Wei, Contact electrification at the solid–liquid transition interface, *Mater. Today*, 2024, **74**, 2–11.

41 Z. Wang, *et al.*, Contact-electro-catalysis for the degradation of organic pollutants using pristine dielectric powders, *Nat. Commun.*, 2022, **13**(1), 130.

42 X. Zhao, Y. Su, A. Berbille, Z. L. Wang and W. Tang, Degradation of methyl orange by dielectric films based on contact-electro-catalysis, *Nanoscale*, 2023, **15**(13), 6243–6251.

43 K. O. Iwuozor, J. O. Ighalo, E. C. Emenike, L. A. Ogunfowora and C. A. Igwegbe, Adsorption of methyl orange: A review on adsorbent performance, *Curr. Res. Green Sustainable Chem.*, 2021, **4**, 100179.

44 D. Afmataj, *et al.*, Adsorption of Reactive Red 120 Dye by Polyamide Nylon 6 Microplastics: Isotherm, Kinetic, and Thermodynamic Analysis, *Water*, 2023, **15**(6), 1137.

45 D. Hu, S. Liu, L. Qi, J. Liang and G. Zhang, A critical review on ultrasound-assisted adsorption and desorption technology: Mechanisms, influencing factors, applications, and prospects, *J. Environ. Chem. Eng.*, 2024, **12**(6), 114307.

46 Z. Wang, *et al.*, A contact-electro-catalysis process for producing reactive oxygen species by ball milling of triboelectric materials, *Nat. Commun.*, 2024, **15**(1), 757.

47 R. Hinchet, *et al.*, Transcutaneous ultrasound energy harvesting using capacitive triboelectric technology, *Science*, 2019, **365**(6452), 491–494.

 This journal is © The Royal Society of Chemistry 2026